

# Identifying the population of stable $\nu_6$ resonant asteroids using large databases

V. Carruba<sup>1\*</sup>, S. Aljbaae<sup>2</sup>, R. C. Domingos<sup>3</sup>, M. Huaman<sup>4</sup>, B. Martins<sup>1</sup>.

<sup>1</sup>São Paulo State University (UNESP), School of Natural Sciences and Engineering, Guaratinguetá, SP, 12516-410, Brazil

<sup>2</sup>National Space Research Institute (INPE), Division of Space Mechanics and Control, C.P. 515, 12227-310, São José dos Campos, SP, Brazil

<sup>3</sup>São Paulo State University (UNESP), São João da Boa Vista, SP, 13876-750, Brazil

<sup>4</sup>Universidad tecnológica del Perú (UTP), Cercado de Lima, 15046, Perú

Accepted 2022 ... . Received 2022 ... ; in original form 2022 March 30

## ABSTRACT

Large observational surveys, like those that will be conducted at the Vera C. Rubin Observatory, are expected to discover up to one million new asteroids in the first year of operation. This will more than double the database of known asteroids in a very short time. New methods and techniques will be needed to handle the large influx of data. Here, we tested some of these new methods by studying the population of asteroids on stable orbits inside the  $\nu_6$  secular resonance. This resonance is one of the strongest mechanisms for destabilizing the orbits of main-belt bodies and producing Near-Earth Asteroids (NEAs). Yet, stable orbital configurations where the asteroid pericenter is either aligned or anti-aligned with that of Saturn exist inside the resonance. The population of stable  $\nu_6$  resonators is now the largest population of asteroids in stable orbits inside a secular resonance. Here we obtained the largest sample of asteroids' proper elements ever used for this problem. Clustering methods and the use of machine learning algorithms permitted the identification of the known asteroid families crossed by the  $\nu_6$  resonance and of two entirely new groups: the Tiffanykapler and the 138605 QW177 families. The Tiffanykapler family is the first young asteroid family ever found in a linear secular resonance, with an age of  $3.0 \pm 1.2$  Myr and an ejection velocity field parameter of  $V_{EJ} = 15^{+6}_{-3}$  m/s. We identify a population of high-eccentricity objects around the Tina family that may be the first example of an asteroid family "resonant halo".

**Key words:** Methods: statistical—Methods: data analysis—Minor planets, asteroids: general.

## 1 INTRODUCTION

Linear secular resonances occur when we have a commensurability between the frequency of precession of an asteroid perihelion,  $g$ , or node,  $s$ , and that of a planet. The  $\nu_6$  occurs when there is a commensurability between the frequency  $g$  of an asteroid and the  $g_6$  frequency of Saturn. This resonance is important for the effect it has on the orbital distribution of asteroids: since it is a pericenter resonance, it can increase most asteroids' eccentricities to planet-crossing levels while keeping their inclinations approximately constant. It can, therefore, destabilize most of the bodies that interact with it, and it is a major source of NEAs through Yarkovsky effect (Bottke et al. 2000). Finally, in the central main-belt, between the 3-1 and 5-2 mean-motion resonances with Jupiter, it separates the population of highly inclined asteroids from the more numerous low-inclination ones (Carruba 2010b).

While most of the asteroids interacting with the  $\nu_6$  secular resonance are dynamically unstable on timescales of a few Myr or less, islands of dynamical stability can be found in-

side the resonance itself. (Yoshikawa 1987), (Knezević et al. 1991), (Morbidelli & Henrard 1991) and (Morbidelli 1993) used a Hamiltonian technique to study the dynamics and topology of the phase space of linear secular resonances in detail. The dynamics of the  $\nu_6$  secular resonance is characterized by the libration or circulation of the resonant angle  $\sigma = \varpi - \varpi_6$ , with  $\varpi$  the longitude of pericenter of the asteroid and  $\varpi_6$  that of Saturn. If the asteroid is outside the resonance, the resonant angle will vary continuously between  $0^\circ$  and  $360^\circ$ . In a  $\nu_6$  librating state the resonant angle will oscillate around an equilibrium point, which can either be  $0^\circ$  or  $180^\circ$ . In the first case, we have an "aligned libration", since the pericenters of both Saturn and the asteroid are pointing in the same direction. For the second case, we have an "anti-aligned libration", and the two pericenters point in opposite directions. Examples of the time behavior of the resonant angle of real asteroids in circulating, switching, anti-aligned, and aligned libration states are shown in figure (1).

Anti-aligned libration is more common near the planet's orbit, and, indeed, is more common in the central and outer main-belt. Carruba & Morbidelli (2011) identified the first case of an asteroid family completely made of as-

\* E-mail: valerio.carruba@unesp.br

teroids in anti-aligned libration states, that of 1222 Tina. (Carruba et al. 2014) later identified the case of the Euphrosyne family, with the second-largest population of asteroids in such states. Finally, (Huaman et al. 2018) extended this analysis to the whole main-belt, and, apart from identifying the case of the 329 Svea family, the third asteroid family in terms of a population of asteroids in  $\nu_6$  anti-aligned states, found the first seven asteroids in aligned states of the same resonance.

In this work, we are interested in further extending the analysis carried out in previous works, by identifying more asteroids affected by the  $\nu_6$  resonance. According to Jones et al. (2015), the catalogs produced by the Vera C. Rubin surveys will increase the known number of tiny bodies in the Solar System by a factor of 10-100 times among all populations, with  $\simeq 1$  million additional asteroid discoveries projected in the first year of operations. New methods will be needed to handle such a massive amount of data, and applications of machine learning (*ML*) software development are currently under development and will increase in the future. The main goal of this paper is to investigate the use of new methods for old problems, like image identification and clustering methods.

For this purpose, we first acquired the largest sample of asteroids' proper elements for numbered and multi-opposition asteroids ever used for this problem with methods described in section (2). Images of the time behavior of asteroid resonant angles are then automatically identified using an Artificial Neural Network (*ANN*) approach, developed by Carruba et al. (2021b) (section (3)). The stability of the orbits in aligned and anti-aligned librating states identified by the *ANN* approach is then studied when non-gravitational forces are considered in section (4). The effect of local dynamics is then studied using dynamical maps of synthetic proper elements in section (5). Asteroid groups among the population of numbered asteroids in anti-aligned libration states are then identified using the Hierarchical Clustering Method (HCM) (Bendjoya & Zappalà 2002) in section (6). Extension in domains of multi-opposition asteroids of the newly identified groups and a study of the families' physical properties are discussed in section (7). In section (8) we date the newly discovered groups using methods based on time-reversal numerical simulations. Constraints on the initial ejection velocity field of the 12988 Tiffanykapler family are discussed in section (9), while section (10) deals with explaining the albedo distribution and high eccentricity population of the Tina asteroid family. Finally, the scientific importance of the new database and the newly identified asteroid groups are discussed in our conclusion, in section (11).

## 2 SELECTING THE POPULATION OF LIKELY $\nu_6$ RESONATORS

To identify the population of  $\nu_6$  resonators, first, we need to select the asteroids most likely to be affected by this resonance. For this purpose, we use the criterion described in (Huaman et al. 2018): we compute the value of  $\sigma = \varpi - \varpi_6$  for all asteroids of interest, and select those for which:

$$-3.5 \leq \frac{d\sigma}{dt} \leq 3.0 \text{ arcsec/yr.} \quad (1)$$

As discussed in (Huaman et al. 2018), these are the bodies that are more likely to be in aligned or anti-aligned librating states of the resonance, according to the analytical model revised in (Huaman et al. 2018). We applied this criterion to all the numbered asteroids for which proper elements and frequencies are available at the Asteroid Families Portal *AFP* (“<http://asteroids.matf.bg.ac.rs/fam/index.php>”; Radović et al. (2017)), i.e., those with an identification up to 523584, which yielded a sample of 4875 asteroids likely to be affected<sup>1</sup>.

Osculating elements are available for an additional 83427 asteroids, up to the identification of 607011 at the *AFP*. For these objects, we first computed proper elements using the Knežević & Milani (2003) approach, also described in Carruba (2010b), and then applied equation (1) to select the likely candidates. This method provided an additional sample of 1350 asteroids that can interact with the  $\nu_6$  resonance. Finally, *AFP* also reports proper elements for a sample of 285861 multi-opposition asteroids. By applying our selection criteria, we obtained an additional population of 3779 asteroids likely to interact with the  $\nu_6$  resonance.

## 3 ANN IDENTIFICATION OF RESONANT ORBITS

The whole sample of asteroids potentially affected by the  $\nu_6$  resonance is 10004. To identify the population of aligned and antialigned asteroids, we first used the approach described in Carruba et al. (2021b), which is a five-step process: first, we integrate the asteroid orbits under the gravitational influences of all planets, then we compute the time-series of the  $\nu_6$  resonant argument, images of these time-series are obtained for each asteroid. The *ANN* model is trained on a training set of labeled image data and, finally, predictions of the labels for a set of test images, usually 50 at a time, are obtained and confirmed by visual inspection by all authors independently.

For this task, we used the *ANN* model described in Carruba et al. (2021b), which is a four-layer neural network with a flatten, inner, hidden, and output layers. Interested readers can find more information in the cited paper. An example of the outcome of this approach is shown in figure (7) of Carruba et al. (2021b). The application of these methods lead to the identification of 30 asteroids in aligned resonant configurations, 9 of which are among the multi-opposition population, and 1713 asteroids in anti-aligned configurations,

<sup>1</sup> Synthetic proper elements as computed with the method of Knežević & Milani (2003) are not very appropriate to study asteroids in secular resonances. For these objects, resonant proper elements, as discussed in Morbidelli (1993) and Carruba & Morbidelli (2011), should rather be used. However, since many of the asteroid families interacting with the  $\nu_6$  secular resonances are crossed by it, and since resonant elements are not usually used for non-resonant asteroids, in this work we will use synthetic proper elements to identify resonant candidates and asteroid groups. Past experiences showed that for family identification, despite differences in proper  $e$  values, results obtained in domains of synthetic and resonant proper elements are fairly similar (Carruba & Morbidelli 2011; Carruba et al. 2014). The special case of the Tina asteroid family where the use of synthetic proper elements may overestimate the real value of proper  $e$  will be treated in section (10).

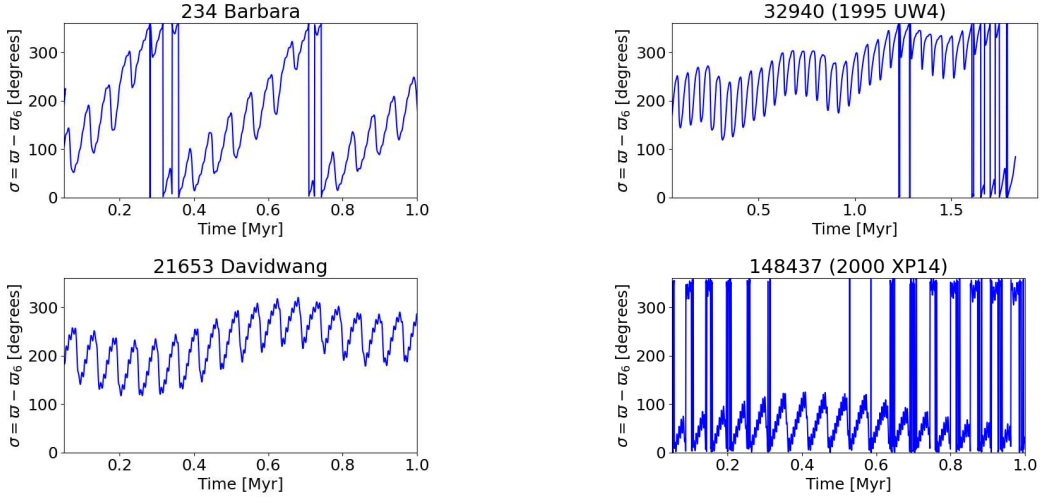


**Figure 1.** Time behavior of the resonant angle  $\omega - \omega_6$  for an asteroid in a circulating orbit (top left panel), in a switching orbit (top right panel) in an anti-aligned orbit (bottom left panel) and in an aligned orbit (bottom right panel).

667 of which among the multi-opposition asteroids. The long-term stability of these orbits when non-gravitational forces are accounted for will be discussed in the next section.

#### 4 EFFECTS OF NON-GRAVITATIONAL FORCES

So far, we analyzed the asteroids' orbits in a purely conservative scenario. Here, we investigate the long-term stability of the objects found in aligned and antialigned states when non-gravitational forces like the Yarkovsky effect are considered. For this purpose, we integrate the population of librating asteroids with *SWIFT – RMVSY*, a symplectic integrator modified to account for the diurnal and seasonal version of the Yarkovsky effect (Brož 1999). We created two sets of clones of these objects, one with a spin obliquity of  $+90^\circ$  and one with  $-90^\circ$ . The prograde particles will maximize the Yarkovsky drift and move towards larger values of semi-major axis, while the retrograde particles will move toward lower values of  $a$  at the maximum possible rate. We neglected in this simulation the YORP effect, which could alter the spin obliquity and asteroid period, and collisions, which could also affect these quantities. We use sizes obtained from the asteroid absolute magnitudes assuming an albedo  $p_V$  of 0.12, which divides C-complex from S-complex objects and can be assumed to be a reasonable compromise between the two. For the other key parameters of the Yarkovsky force, we used a density and a bulk density of  $1500 \text{ kg m}^{-3}$ , a thermal conductivity  $K$  of 0.01  $\text{W}/(\text{m K})$ , a specific heat  $C_P = 680 \text{ J kg}^{-1} \text{ K}^{-1}$  a Bond albedo of 0.05, and an infrared emissivity  $\epsilon$  of 0.95. The test particles were integrated over 5 Myr over the gravitational influence of all planets and the time behavior of the  $\nu_6$  resonant angle was verified for both clones.

If both clones remained in a librating configuration over the length of the simulation, the librating behavior was deemed as confirmed. However, if one of the clones escaped from aligned or antialigned libration during the simulation, we dropped the corresponding asteroids from our list of resonant objects. Figure (2) displays the time behavior of the  $\nu_6$  resonant angle

for particles that escaped aligned libration (left panel) and antialigned libration (right panel) because of the Yarkovsky force.

Out of 30 asteroids in possible aligned configurations, only 15 passed this test, and only one of them was a multi-opposition asteroid. The survival rate was much higher for antialigned orbits: out of 1713 asteroids, only 44 escaped the antialigned configuration because of non-gravitational forces, i.e., 2.57%. This difference in behavior between aligned and antialigned orbits is caused by the fact that an antialigned orbit has to cross the resonance separatrix to become a circulating orbit and be lost because of planetary close encounters. Stable aligned orbits are those of small librating amplitudes. An increase in the libration amplitude caused by planetary perturbations is enough to destabilize the aligned configuration. This explains why aligned orbits are rarer and more unstable when non-gravitational forces are considered. The next section will focus on better understanding the effects of the local dynamics on the confirmed population of stable  $\nu_6$  librators.

#### 5 LOCAL DYNAMICS

The dynamical location of the  $\nu_6$  resonance has been discussed in detail in several prior papers. Interested readers could find more information in Huaman et al. (2018). Here, we briefly revise some basic concepts, using dynamical maps of synthetic proper elements to highlight the local dynamical environment.

Synthetic proper elements are quasi-integral of motions obtained through Fourier analysis of time-series of osculating elements (Knežević & Milani 2003). Here we apply the procedure described in Carruba (2010b) to obtain dynamical maps of synthetic proper elements. Essentially, a grid of initial conditions in a 2-dimensional plane is created, and the test particles are integrated over the gravitational influence of all planets with a symplectic integrator, like, for instance, the *SWIFT – MVSF* mixed-variable symplectic integrator of Levison & Duncan (1994), modified by Brož (1999)

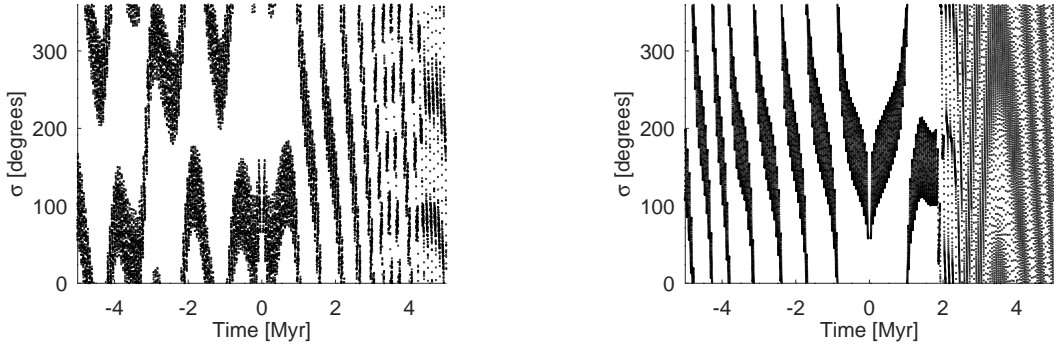


**Figure 2.** Time behavior of the  $\nu_6$  resonant angle for two clones of asteroids that escaped from aligned configuration (asteroid 538256, left panel) and anti-aligned configuration (asteroid 60683, right panel). The time interval from -5 Myr to 0 refers to the evolution of the retrograde clone, while the interval from 0 to 5 Myr displays the behavior of the prograde one.

to allow for online filtering. The four elements not in the bi-dimensional grid are usually taken equal to those of an asteroid of interest, in our case 1222 Tina. The initial conditions and displacements in orbital elements for our maps are shown in table (1). All maps had 35 initial conditions on the x-axis and 60 on the y-axis, for a total of 2100 test particles.

Here we created six maps in the  $(a, \sin(i))$ , and  $(a, e)$  planes, for the inner, central, and outer main-belt. The initial conditions and number of particles for our maps are shown in table (1). Our results are shown in figure (3). Synthetic proper elements for the test particles are shown as black full circles. The populations of numbered asteroids that are on aligned, anti-aligned librating or switching particles (15, 1046, and 362, respectively) are shown as blue, red and yellow full circles. Mean-motion resonances appear as vertical bands with low number-density of asteroids, while secular resonances are inclined bands in the  $(a, \sin(i))$  and  $(a, e)$  domains. The lack of test particles at low eccentricities is an artifact of the process used to generate the dynamical maps.

In the inner main-belt, we have two main agglomerations, one at 2.45 au associated with the Svea asteroid family, and another at lower values of proper  $a$  that follows the lower contours of the unstable region caused by the  $\nu_6$  secular resonance. In the central main-belt, we have the group associated with the 1222 Tina family, scattered asteroids at lower  $a$ , and a population of objects in aligned libration states that follow the upper boundary of the  $\nu_6$  unstable region. In the outer main-belt, we have the group of anti-aligned asteroids associated with the Euphrosyne family.

If we also consider the multi-opposition asteroids, then we have 9 more aligned, 667 antialigned, and 90 switching objects. Our results are displayed on figure (4). Trends previously observed for the numbered objects are mostly confirmed by the multi-opposition population as well, except for aligned asteroids. We only found one multi-opposition asteroid in the outer main-belt, near the 2:1 resonance, whose orbit was stable when the Yarkovsky force was considered: 2015 DP197. In the next section, we aim to identify groups among the antialigned asteroidal population that has been detected so far.

## 6 ASTEROID GROUPS

The Hierarchical Clustering Method (HCM) has been used since the early 90s to identify asteroid families (Bendjoya & Zappalà 2002). The most common variant of the method will look for neighbors of an asteroid in a domain of the  $(a, e, \sin(i))$  proper elements, using a distance metric appropriate for the problem at hand. If the distance between the first asteroid and the second is less than a critical value,  $d_0$ , the second asteroid is assigned to the family membership list and the procedure is then repeated for the second body, until no new members are encountered.  $d_0$  is a free parameter of the method, that depends on the number density of asteroids in a given orbital region. Here we follow the approach of Beaugé & Roig (2001) that defines  $d_0$  as the mean of the minimum distances between all asteroids in the region.

Two useful methods for identifying asteroid families are obtaining family membership versus cutoff and stalactite plots. For the first method, one plots the number of family members as a function of increasing distances, up to values of distances high enough that all asteroids in the orbital region are associated with a given family. In a stalactite diagram, as constructed by Brož & Vokrouhlický (2008), first all the asteroids in a family that includes all the objects in the region are displayed. The cutoff distance value is then reduced and asteroid groups are identified among the population of objects no longer associated with the initial family. The procedure is then repeated for lower and lower values of the distance cutoff. Results are presented in a plane where the families' memberships are shown on the x-axis and the distance cutoff is shown on the y-axis. More details on all these methods and procedures are described in Carruba (2010b).

Our dataset of proper elements is comprised of the numbered asteroids in antialigned states of the  $\nu_6$  resonance. Except for a single object with a semi-major axis beyond the 2:1 mean-motion resonance with Jupiter, in the Cybele region, all the other asteroids can be found in the inner main-belt, for values of  $a$  lower than those of the 3:1 mean-motion resonance with Jupiter ( $a_{3:1} = 2.485$  au), in the central main-belt ( $a_{3:1} < a < a_{5:2}$ , with  $a_{5:2} = 2.826$  au), and in the outer main-belt ( $a_{5:2} < a < a_{2:1}$ , where  $a_{2:1} = 3.279$  au). Table (2) displays the number of asteroids and the values of  $d_0$  for the three regions of interest. We define a family as a group with at least 5 members. In the next section, we will discuss our results for the inner main-belt.

**Table 1.** For each of the six maps shown in figure (3), we report the initial value of the element used in the x-axis, in the y-axis, and the displacement used for the grids in x and y.

Map Id.	Initial el. (1)	Initial el. (2)	Change in el. (1)	Change in el. (2)
1	2.4850 [au]	16 [degrees]	0.0100 [au]	0.125 [degrees]
2	2.4850 [au]	0	0.0100 [au]	0.005
3	2.0800 [au]	0 [degrees]	0.0115 [au]	0.3 [degrees]
4	2.0800 [au]	0	0.0115 [au]	0.005
5	2.8258 [au]	19 [degrees]	0.0107 [au]	0.21 [degrees]
6	2.8258 [au]	0	0.0107 [au]	0.0061

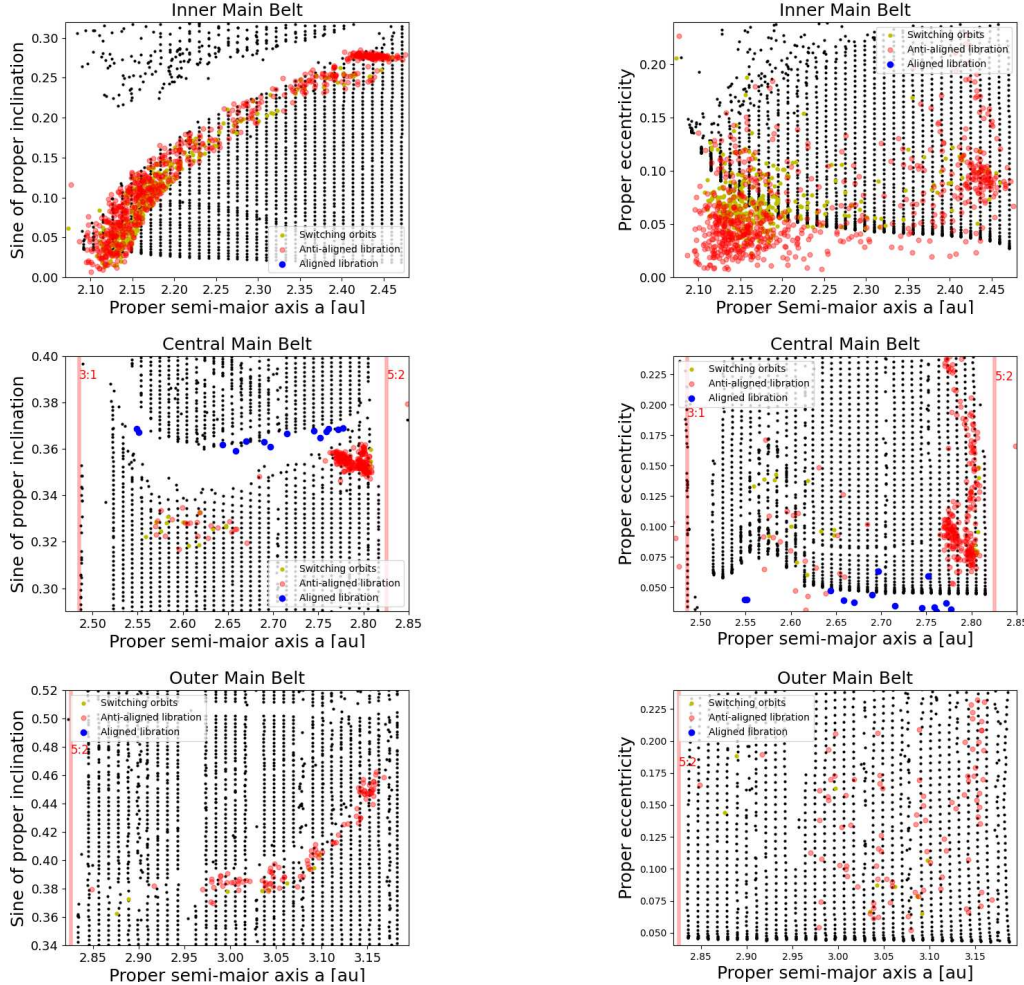


**Figure 3.** Dynamical maps of synthetic proper elements in the  $(a, \sin(i))$  plane (left panels), and in the  $(a, e)$  plane (right panels). The top panels display asteroids in the inner main-belt, the central panels those in the central main-belt, and the bottom panels asteroids in the outer main-belt. Black dots show the orbital location of proper elements for the test particles used in the six simulations. Red full circles identify real asteroids in anti-aligned libration states, blue full circles real asteroids in aligned libration states, and yellow full circles asteroids that alternate phases of libration and circulation.

### 6.1 Inner main-belt

The inner main-belt contains the largest population of asteroids in  $\nu_6$  antialigned resonant states. Two main groups of asteroids are found in this region, one for  $a < 2.30$  au, where most of the asteroidal population is found, and one for higher values, mostly associated with the Svea family, as discussed in Huaman et al. (2018).

The left panel of figure (5) shows a family count plot for groups starting with the Svea family members. As we increase the distance cutoff, several smaller groups are englobed by the main group, as shown by the peaks in the differential increase in the group members (orange line). At  $d_0 = 420$  m/s the Svea family merges with the rest of the population, and from then on essentially all asteroids are linked in a unique group. The

**Table 2.** Number of asteroids on antialigned orbits and cutoff distance  $d_0$  for the inner, central and outer main belt regions.

Main-Belt region	Number of asteroids	Cutoff distance $d_0[m/s]$
Inner	682	160.5
Central	252	69.7
Outer	112	185.5

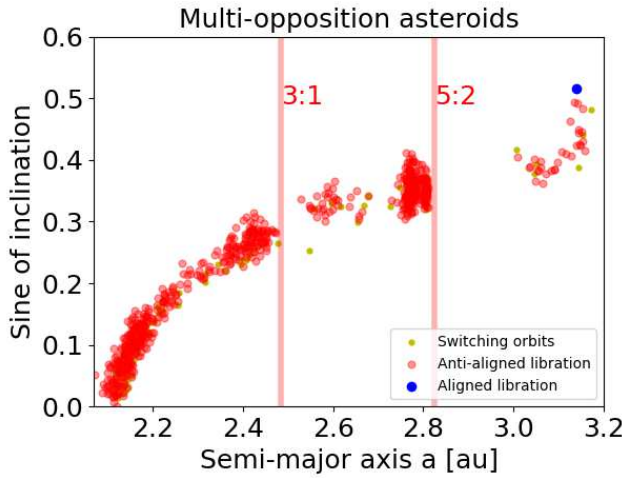


**Figure 4.** An  $(a, \sin(i))$  projection of multi-opposition asteroids (right panel) in aligned, anti-aligned and switching states of the  $\nu_6$  secular resonance. The symbols have the same meaning as in figure (3).

stalactite diagram for this region identifies two main groups: a group around 34804 2001 SP67, associated with the Svea family, and a completely new group in the inner main-belt around 12988 Tiffanykapler. As discussed by [Huaman et al. \(2018\)](#), the Svea family is cut by the  $\nu_6$  secular resonance in two parts and the part near asteroid 329 Svea itself is not in a resonant configuration. This explains why the Svea group's lowest-numbered member is 34804 and not 329 Svea. The new Tiffanykapler group is located at  $a \simeq 2.182$  au and it is not part of any currently known family. The dynamical and physical properties of this new group will be discussed in section (7).

## 6.2 Central main-belt

The main asteroid group in the central main-belt is that of 1222 Tina, and no other group has been identified so far in this region ([Carruba & Morbidelli 2011](#)). This picture is confirmed by the analysis performed in this work. The Tina family essentially coalesces for cutoff values slightly lower than the local distance cutoff  $d_0 = 69.7$  m/s, and only minor groups are merging with the main family at larger cutoffs (see figure (6, left panel). The stalactite diagram confirms this analysis and at the distance cutoff computed for the central main-belt only the Tina family is observed as a group. Concerning previous determinations of the Tina family, however, we identify in this work a population of objects at higher

eccentricities that are not members of the Tina dynamical family (see figure (3, center right panel). No single dynamical group has been identified among this new population, and its nature will be investigated in more detail in section (10).

## 6.3 Outer main-belt

In the outer main-belt, the main family interacting with the  $\nu_6$  resonance is that of Euphrosyne ([Carruba et al. 2014](#)). Figure (7), left panel, shows how the family members increased starting with the lowest numbered asteroid in the inner part of the outer main-belt. The peak observed at 410 m/s occurs when there is the merging with the Euphrosyne family. An analysis of the stalactite diagram for this region identifies two groups: one around 67834 2000 VV53 and another around 138605 2000 QW177. The first one is associated with the Euphrosyne family, while the second is a completely new group, not associated with any currently known asteroid family.

In the next section, we will analyze the physical and dynamical properties of the groups identified in this work.

## 7 NEWLY IDENTIFIED $\nu_6$ GROUPS: PROPERTIES

As a first step, we attempt to extend the membership of identified groups by including multi-opposition asteroids in  $\nu_6$  antialigned resonant states. For this purpose, we use the approaches described in [Carruba et al. \(2020b\)](#) and [Carruba et al. \(2021a\)](#). The groups identified in our previous analysis are used to train a ML algorithm, whose hyper-parameters are first optimized through the use of genetic algorithms ([Chen, P. W. and Wang, J. Y. and Lee H. 2004](#)), according to the procedure described in [Carruba et al. \(2021a\)](#). The best performing algorithm is then used to select the population of multi-opposition asteroids with the proper elements  $(a, e, \sin(i))$  closest to those of the training sample ([Carruba et al. 2020b](#)). These methods will identify asteroids whose proper orbital elements are close to those of the identified families, but they will not identify objects that could have been connected to the family using traditional HCM. Since the orbits of some multi-opposition asteroids are known with some uncertainties, we believe that such a conservative approach is reasonable.

The groups of interest will be then studied using standard HCM in a domain of proper elements for all asteroids, resonant or not, to check for what distance cutoff they connect to other local families. This is important to check for families that are crossed by the  $\nu_6$  resonance and have a population of both resonant and non-resonant members. The limitations of this approach have been discussed in section (2), see footnote

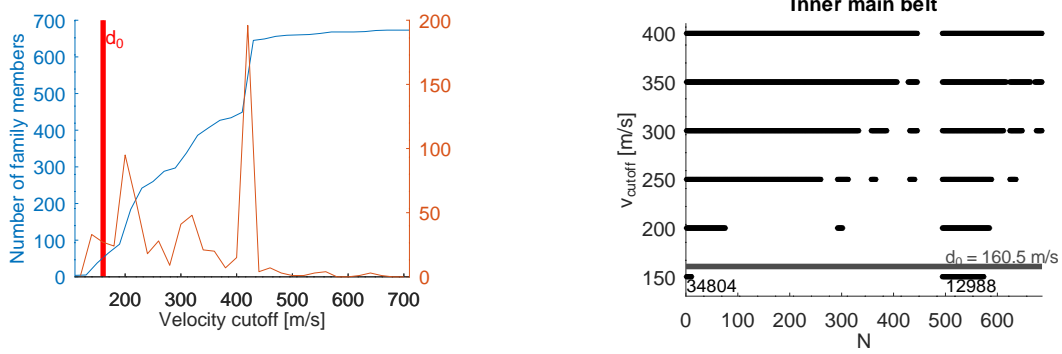


**Figure 5.** On the left panel we show the number of members of the group associated with the lowest numbered asteroid in the inner main-belt, 930 Westphalia, as a function of the distance cutoff (blue line). The orange line shows the differential increase in the group members for each increase in the cutoff value. The thick red line displays the critical cutoff value for the inner main-belt. On the right panel, we display a stalactite diagram for the same region. Black full dots identify members of asteroid groups at various values of the distance cutoff. The critical value for this region is shown as a thick horizontal line. The identified clusters are identified by the lowest id number among their members.

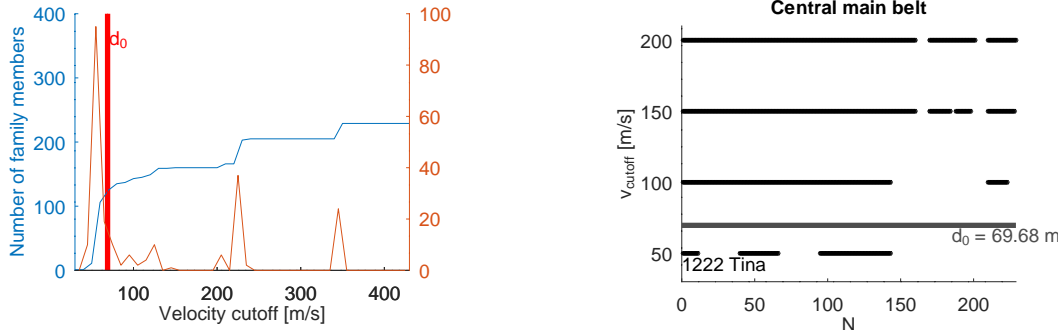


**Figure 6.** The same as in figure (5), but for the central main-belt. We used 1222 Tina as a possible parent body to generate both panels.

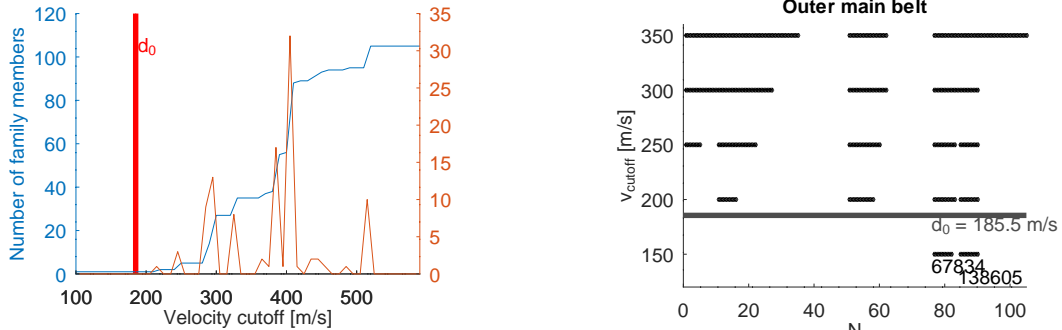


**Figure 7.** The same as in figure (5), but for the outer main-belt. The lowest numbered asteroid in the outer main-belt, 3939 Huruhata is not associated with any known dynamical groups, which explains why no peak is observed at a cutoff equal to  $d_0$ .

(1)). Yet, it is a necessary step to see if the newly discovered families extend beyond the limits of stable orbits in the  $\nu_6$  resonance.

Finally, we looked to see if the taxonomic traits of resonant group members were consistent with a common ancestor. We use the method of DeMeo & Carry (2013) to obtain taxonomical information for asteroids listed in the Sloan Digital Sky Survey-Moving Object Catalog data (SDSS-MOC4; Ivezić et al. (2001)). We also look for bodies in the WISE and NEOWISE, AKARI, or IRAS databases that have geometric albedo values (Masiero et al. 2012; Usui et al. 2011; Ryan & Woodward 2010). Under the assumption of an ori-

gin from a homogeneous parent body, all members of a family should have compatible values of taxonomy and albedo.

We start our analysis by looking at resonant groups in the inner main-belt.

## 7.1 Inner main-belt

Two main groups were identified in the inner main-belt, that of 34804, associated with the Svea asteroid family, and the new Tiffanykapler group at lower values of  $a$ . We first extended these two groups in the domain of resonant multi-opposition asteroids. The best perform-

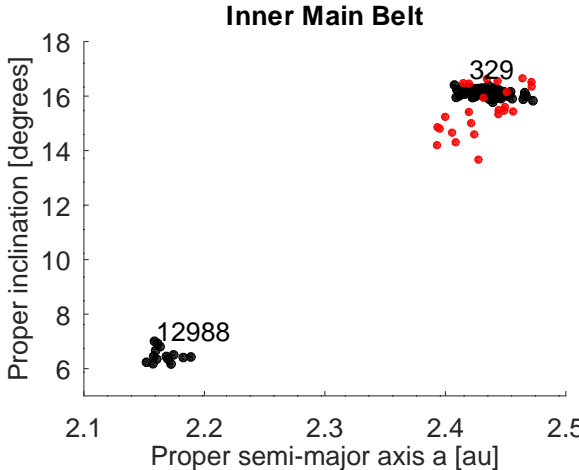


**Figure 8.** The  $(a, \sin(i))$  distribution of the identified numbered (black full circles) and multi-opposition (red full circles) members of resonant groups in the inner main-belt.

ing algorithms after five generations were an Extra Tree and a Decision Tree classifier. For the Extra Tree classifier, we had these hyper-parameters: `bootstrap=False`, `criterion="gini"`, `max_features=0.7`, `min_samples_leaf=13`, `min_samples_split=17`, `n_estimators=100`. For the case of the Decision Tree estimator, we had: `max_depth=7`, `min_samples_leaf=14`, `min_samples_split=19`. Interested readers can find more information on the meaning of the hyper-parameters name and their effect on the Scikit-learn documentation page (<https://scikit-learn.org/stable/>), Pedregosa et al. (2011)), or in Carruba et al. (2021a). 24 new possible members of the Svea family were found by these methods, while no multi-opposition asteroid in our database appears to be a possible member of the Tiffanykapler group (see figure (8)).

The HCM analysis of these two groups shows that the Svea resonant group connects with a nearby family for a cutoff of 150 m/s, while the Tiffanykapler joins the Flora family at a distance of 110 m/s. Both groups are fairly isolated and identifiable in proper elements domains. Finally, no SDSS taxonomical information is available for any members of the two resonant groups. Albedo information is available only for 13 members of the Svea resonant group and for 1 of the Tiffanykapler. The albedo of 12 members of the Svea group is below 0.08, and compatible with that of the family, which belongs to the C-complex. One object, 59626 1999 JA75 has an albedo of 0.187 and could be an interloper. The only object with an albedo value in Tiffanykapler is 65010 2002 AR82, with  $p_V = 0.457$ . The largest object in this group is 12988 Tiffanykapler itself, with an estimated diameter of 1.45 km, using this albedo value and the asteroid absolute magnitude of 15.82. Other group members are all smaller than 1.0 km in diameter.

## 7.2 Central main-belt

The main group of asteroids in the antialigned configuration in the central main-belt is the Tina family (Carruba & Morbidelli 2011). The best performing algorithm to extend this family in the domain of multi-opposition asteroids was a Decision Tree classifier with `max_depth=10`,

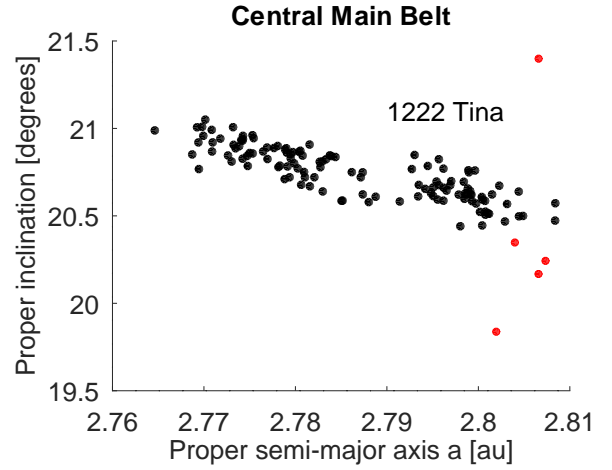


**Figure 9.** The  $(a, \sin(i))$  distribution of the identified numbered (black full circles) and multi-opposition (red full circles) members of the Tina asteroid family in the central main-belt.

`min_samples_leaf=4`, and `min_samples_split=5`. Five multi-opposition asteroids were found to be likely members of the Tina family. Their orbital location is shown in figure (9).

Because of its orbital location, entirely located in a stable island in the unstable orbital region caused by the  $\nu_6$  secular resonance, the Tina family is rather isolated and quite distinguishable from the surrounding families. All the asteroids in the stable island are connected to the family by HCM for a cutoff distance of 130 m/s, and the group merges with nearby families only at a distance of 280 m/s. A population of 44 asteroids at higher eccentricities than those of the family (see figure (3), center-right panel) has been identified in this work for the first time. Its dynamical evolution and possible origin from the Tina family is an interesting topic for future research.

SDSS taxonomy is available for only one object, 81986 2000 QQ123, whose X-type is compatible with the taxonomy of 1222 Tina. 42 asteroids have values of albedo, mostly provided by the NEOWISE database. The albedo distribution of these asteroids is rather difficult to interpret. The range covered by the mean value, plus or minus one standard deviation, is  $0.137 \pm 0.044$ . However, the albedo of 1222 Tina, 0.202 itself is outside this range, and there are six asteroids with albedos lower than the values in the range. This problem was already noticed in Carruba & Morbidelli (2011), and the new data confirmed this trend. Figure (10) displays a histogram of the albedo values. The unusual albedo values, generally quite large for an X-type asteroid family, and their unusual distribution will be investigated later on in this paper.

## 7.3 Outer main-belt

Two groups have been identified in the outer main-belt, those of 67834 2000 VV53, associated with the Euphrosyne family, and the new group of 138605 QW177. The best-performing algorithms for connecting these groups to the multi-opposition population were an Extra Tree Classifier with the same hyper-parameters as in section (7.1) and a Gaussian Naive Bayes with no optimized hyper-parameter. Neither identified new members of the two groups among the 24 multi-

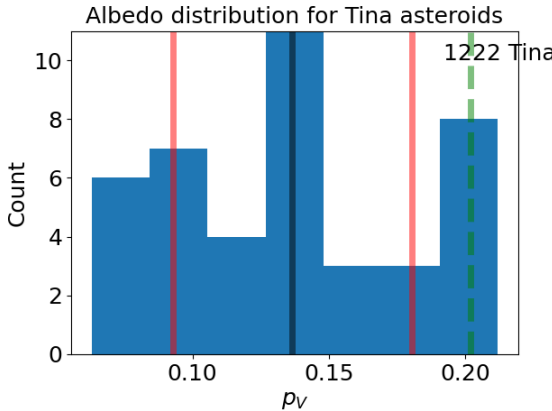


**Figure 10.** An histogram of albedo values in the Tina family. The black vertical line show the mean albedo value, while the vertical red lines shows the limits of the albedo range, as defined in the text. The green vertical dashed line displays the albedo of 1222 Tina.

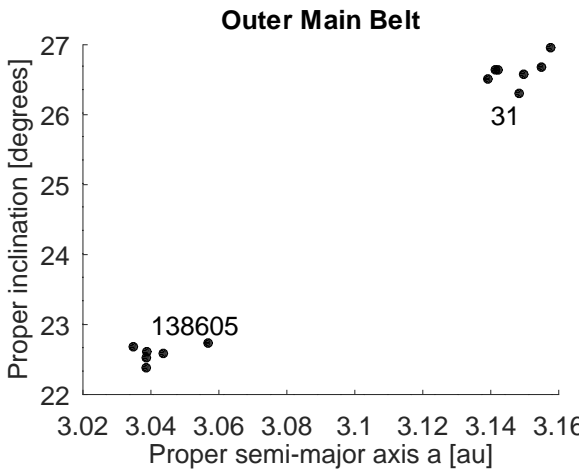


**Figure 11.** The  $(a, \sin(i))$  distribution of the identified numbered members (black full circles) of resonant groups in the outer main-belt.

opposition asteroids in the region. The  $(a, \sin(i))$  orbital distribution of the two groups is displayed in figure (11).

The HCM analysis of these two groups shows that the first one connects to the surrounding Euphrosyne family already at a cutoff of 30 m/s, while the other group is rather isolated, only connecting to nearby families for the rather large value of the cutoff of 130 m/s. No SDSS information is available for any members of both groups. NEOWISE albedo information is available for 2 members of the Euphrosyne and 4 members of the 138605 group. All six asteroids have albedos lower than 0.08, compatible with a C-complex taxonomy, which is consistent with the case of the Euphrosyne family. The largest member of the 138605 group is 417866 2007 LY33, with an estimated diameter of 6.077 km. The remaining asteroids in the group have estimated diameters lower than 5.2 km.

## 8 DATING THE NEW RESONANT FAMILIES

Having identified two new possible asteroid groups, here we attempt to infer information about their ages. Both the 12988 and 138605 are fairly small groups, with 14 and 6 members each. Dating methods using the slope of the V-shape of family members in the  $(a, 1/D)$  domain (Spoto et al. 2015), or the Yarko-Yorp approach of Vokrouhlický et al. (2006a), among others, will not work for such groups, because of small number statistics issues. However, both groups are ideally suited for being studied with methods designed for young clusters, like the Backward Integration Method (BIM, Nesvorný et al. (2002)) and the Close Encounters Method (CEM, Pravec et al. (2010))

In the BIM method, from time-reversal numerical simulations, past discrepancies in the longitudes of the pericenter  $\varpi$  and node  $\Omega$  of family members with respect to those of the claimed parent body are obtained. These differences should converge to values approaching zero at the time of family formation. For asteroids inside the  $\nu_6$  secular resonance, where  $\varpi$  is in a locked mechanism with the longitude of pericenter of Saturn, the method can only use convergence in  $\Omega$ , but the principle remains the same.

The CEM approach works by integrating into the past multiple clones of the parent body and of the other family members. Close encounters that occur at low relative distances and speeds between two clones are recorded, and the median value of these times is used to estimate the asteroid pair's age. The cutoff values for relative distances and speed of the encounters are defined in terms of the Hill's radius and escape velocity of the primary body. More technical details on both these methods, as implemented by our group, can be found in the methods section of Carruba et al. (2020a)<sup>2</sup>.

Figure (12) displays the past convergence of differences in  $\Omega$  with respect to the possible parent body of members of the 12988 Tiffanykapler (left panel) and 138605 QW177 (right panel) groups. Since we are neglecting in this simulation the effect of non-gravitational force, convergence should occur to within  $\pm 60^\circ$ . We show these levels as horizontal dashed lines in the figure. We find a possible solution for the 12988 group in the time range from 3.3 to 6.5 Myr ago (see figure (12), left panel, vertical dashed lines). No solution was found for the 138605 group. According to these results, 12988 Tiffanykapler could be the first young asteroid family to ever be found in a linear secular resonance state.

To confirm this exciting hypothesis, we turn our attention to the results from the CEM approach. Figure (13) shows an example of how statistics of close encounters in the past can be used to estimate the age of an asteroid pair. The median value of the distribution is used to obtain the age estimate, while the errors are obtained by considering the 5th and 95th percentiles. For the pair shown in the figure the age was of  $3.665^{+2.929}_{-3.388}$ , and there were 95 encounters that satisfied our selection criteria in this simulation. While all the asteroid

<sup>2</sup> As discussed in Carruba et al. (2020a), fission pairs may occur inside relatively young asteroid families. We looked for candidate pairs, characterized by relative distance in proper elements, as computed with equation (4) in Carruba et al. (2020a), of less than 5 m/s, and a mass ratio (see equation (5) in Carruba et al. (2020a)) of less than 0.3, in both the 12988 and 138605 groups. No candidate pair was identified in either families.

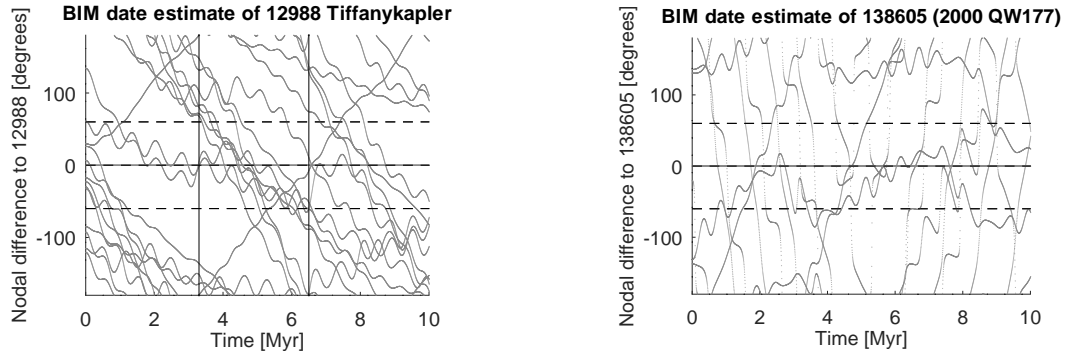


**Figure 12.** Past convergence of the differences in  $\Omega$  with respect to the alleged parent body for members of the 12988 Tiffanykapler (left panel) and 138605 QW177 (right panel) groups.

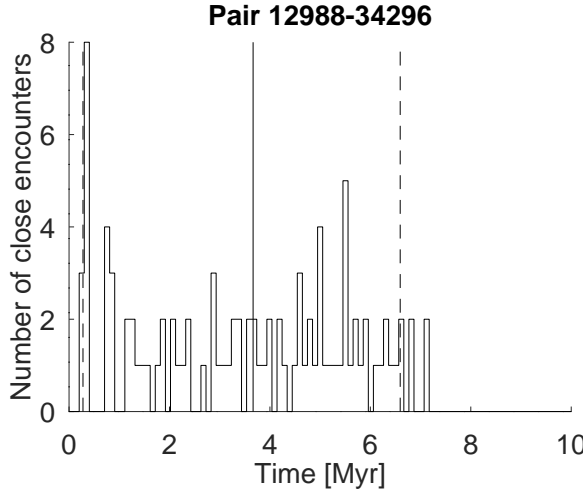


**Figure 13.** An example of statistics of close encounters between 12988 and 34296, a member of the Tiffanykapler group. The vertical line shows the median value of the age estimate, while the vertical dashed lines display the 5th and 95th percentiles of the distribution, used to estimate the error on the pair age.

pairs in the Tiffanykapler groups have significant statistics of close encounters, all with ages compatible with the range found from BIM, most asteroid pairs in the 138605 groups have less than 10 encounters over the 10 Myr length of the simulation. Both results from BIM and CEM suggest that either the 138605 is older than 10 Myr, or that it may be an artifact of the HCM procedure described in section (7).

Our results for the pairs in the 12988 Tiffanykapler group are summarized in Table (3). If we take as an estimate of the error the larger value between the upper and lower age estimate range, which, for the first asteroid pair would mean taking 3.388 Myr as an estimate of the standard deviation  $\sigma_1$  for the age  $x_1$ , then the asteroid age can be estimated using the weighted mean formula:

$$\bar{x} = \frac{\sum_{i=1}^{n_{pairs}} \left( \frac{x_i}{\sigma_i} \right)}{\sum_{i=1}^{n_{pairs}} \frac{1}{\sigma_i^2}}, \quad (2)$$

**Table 3.** Age estimates for pairs in the 12988 Tiffanykapler cluster obtained with CEM.

Asteroid Id.	Number of enc.	Age [Myr]
34296	95	$3.665^{+2.929}_{-3.388}$
65010	124	$3.273^{+3.519}_{-3.060}$
112247	68	$3.540^{+3.260}_{-2.685}$
131528	98	$3.163^{+3.521}_{-2.547}$
149823	85	$2.893^{+3.461}_{-2.547}$
227780	82	$2.993^{+3.433}_{-2.830}$
340833	88	$3.788^{+2.788}_{-3.618}$
380442	89	$2.614^{+3.157}_{-2.377}$
389850	83	$3.192^{+3.396}_{-3.020}$
408140	45	$3.829^{+2.919}_{-3.571}$
464017	73	$2.491^{+4.095}_{-2.465}$
483384	92	$2.380^{+3.735}_{-2.005}$
495612	55	$4.132^{+2.855}_{-3.976}$

where  $n_{pairs}$  is the number of asteroid pairs, in our case 13. The standard error of the weighted mean is then given by:

$$\sigma_{\bar{x}} = \sqrt{\frac{1}{\sum_{i=1}^{n_{pairs}} \frac{1}{\sigma_i^2}}}. \quad (3)$$

Using the data from table (3) we obtain an estimated age for the 12988 Tiffanykapler family of  $3.05 \pm 1.15$  Myr. This makes the Tiffanykapler the first ever identified young asteroid family inside a linear secular resonance. In the next section, we will investigate what information can be obtained from the resonant configurations of these two groups.

## 9 SECULAR CONSTRAINTS ON THE INITIAL EJECTION VELOCITY FIELD OF THE 12988 TIFFANYKAPLER FAMILY

In this section we will investigate what constraints can be obtained on the ejection velocity field of the Tiffanykapler family from its secular nature. Since there are only six members in the 138605 QW177 group, these statistical methods cannot be applied to this family. As discussed in

Carruba & Morbidelli (2011), at the simplest level of perturbation theory the quantity:

$$K'_2 = \sqrt{1 - e^2}[1 - \cos(i)], \quad (4)$$

is preserved for asteroids in the  $\nu_6$  resonance in the conservative case. Simulations performed by Carruba & Morbidelli (2011) showed that this quantity is also preserved when non-gravitational forces are considered. Current values of the  $K'_2$  quantities for members of the Tiffanykapler family are displayed in the left panel of figure (14).

The preservation of the original values of  $K'_2$  permits to estimate the initial ejection velocity field with a method not generally available for non-resonant families (Vokrouhlický et al. (2006b), see also the review in Carruba et al. (2018)). First, we assume that asteroids are ejected with an isotropic ejection velocity field whose standard deviations  $V_{SD}$  are proportional to the asteroid size via the parameter  $V_{EJ}$ , via the relationship:

$$V_{SD} = V_{EJ} \cdot \left( \frac{5 \text{ km}}{D} \right), \quad (5)$$

where  $D$  is the asteroid diameter in km. While this method may not provide an accurate measure of the ejection velocities for asymmetric fields, it can provide useful constraints on its magnitude. We create multiple synthetic asteroid families with various  $V_{EJ}$  parameter values, calculate their  $K'_2$  quantities, and determine which of the simulated families is best compatible with the currently observed  $K'_2$  distribution. We can utilize a  $\chi^2$ -like variable defined as equation (6) to quantitatively test this:

$$\chi^2 = \sum_{i=1}^{N_{int}} \frac{(q_i - p_i)^2}{q_i}. \quad (6)$$

$N_{int} = 6$  is the number of intervals used to obtain the histogram of the  $K'_2$  distribution.  $q_i$  and  $p_i$  are the numbers of real and simulated objects in the  $i$ -th interval, respectively. Once values of  $\Delta\chi^2 = \chi^2 - \chi^2_{min}$  are obtained, where  $\chi^2_{min}$  is the minimum value of  $\chi^2$ , the  $\chi^2$  probability distribution function can be used to determine the 97.5% confidence level (see Carruba et al. (2018) for a more in-depth description of this method). Our results are shown in the right panel of figure (14). Our analysis yields a value of  $V_{EJ} = 15^{+6}_{-3}$  m/s.

## 10 TINA FAMILY: ALBEDO DISTRIBUTION AND HIGH ECCENTRICITY POPULATION

Two open questions were raised by our investigation of the Tina family: the unusual albedo distribution of Tina asteroids (see figure (10)) and the origin of the high eccentricity population (see figure (3), panel 4).

To answer the first question, we divided the sample of objects with albedo information in two parts, those with values of  $a$  less than that of 1222 Tina, and those with larger values. Since the family center of mass is essentially located at the orbit of Tina, the first population corresponds to the left side of the family V-shape in the  $(a, 1/D)$  domain, as defined in Spoto et al. (2015), while the second belongs to the right side. Then, we further divide asteroids according to their albedo,

with a first sample with  $pv < 0.12$ , usually associated to a C-complex taxonomy, and a second sample with  $pv > 0.12$ , usually related to S-complex compositions. The percental distribution of these four groups are shown in figure (15).

The distributions of low- and high albedo objects on the left and right side of the Tina family are very compatible. A two-sample Kolmogorov-Smirnoff test (or K-S test, (Smirnov 1939)) dismissed the probability of the two distributions being different to the null hypothesis level of 5%. This result suggests that a common origin should be found for both populations. The Tina family may be characterized by an unusually broad distribution of albedo values, not commonly observed in other parts of the main-belt for X-type families.

Concerning the high-e Tina asteroidal population, as discussed in section (2), resonant proper elements are more appropriate for the case of resonant asteroids. Two approaches for obtaining resonant elements were discussed in Carruba & Morbidelli (2011), one based on Fourier analysis of the equinoctial elements  $(e \cos(\varpi - \varpi_6), e \sin(\varpi - \varpi_6))$ , where the second frequency of largest amplitude is identified as the resonant proper frequency  $g_\sigma$ , and its associated amplitude is the resonant eccentricity  $e$ . The second method is based on the conservation of the  $K'_2$  quantity and on taking as proper  $e$  the value of  $e$  when  $\sigma = 180^\circ$  and  $\frac{d\sigma}{dt} > 0$ . As in Carruba & Morbidelli (2011), here we will use the first approach, since the second method does not provide values of the proper frequency  $g_\sigma$ .

Our results for both synthetic and resonant elements are shown in figure (16). Quite interestingly, values of resonant proper  $e$  are significantly smaller than those of the synthetic  $e$ . The bulk of the high-e population it is still not connected to the Tina dynamical family even if we used HCM in the new domain of resonant proper elements. But, it connects to the family at a higher cutoff of 100 m/s. This behavior is consistent with what is observed for other families halos. The concept of an asteroid family halo was first introduced by Brož & Morbidelli (2013) and refers to an extended population of asteroids that is not recognized as part of a family by standard HCM approaches, but it is quite likely to have been produced by the collision event that produced the dynamical family. Experience with other families halos shows that many objects in these population may connect to the family core when higher values of cutoff are considered (Carruba et al. 2013). This high-e population of Tina-like asteroids may be the first example of a “resonant halo” ever to be identified. The main difference with respect to the halo of non-resonant families being that the dimensions of this halo are limited by the available area in the stable island. One object, 599705 (2010 TD202), is very close to the resonant separatrix and becomes unstable on timescales of a few Kyr when time-reversal simulations are carried out. This can be an example of observable dynamical erosion of an asteroid family in action, as defined in Carruba (2010a).

## 11 CONCLUSIONS

The main goal of this paper was to update our knowledge on the population of asteroids in stable states **inside** the  $\nu_6$  secular resonance, and to identify new asteroid groups among this population. As discussed in Carruba et al. (2018), asteroid groups interacting with secular resonances are important

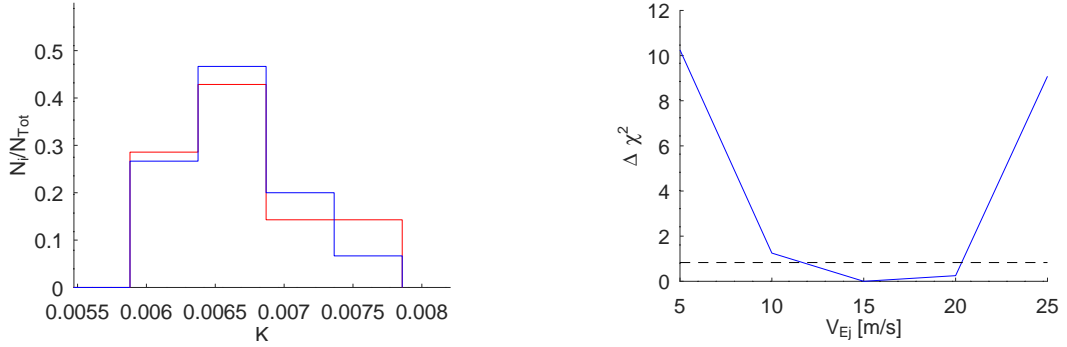


**Figure 14.** Left panel: a normalized histogram of the distribution of  $K'_2$  values for members of the Tiffanykapler family (red line) and of the simulated asteroid family that best fit the data (blue line). Right panel: Dependence of  $\Delta\chi^2$  as a function of the  $V_{\text{EJ}}$  parameter. The 97.5% confidence level limit is identified by the horizontal dashed line.

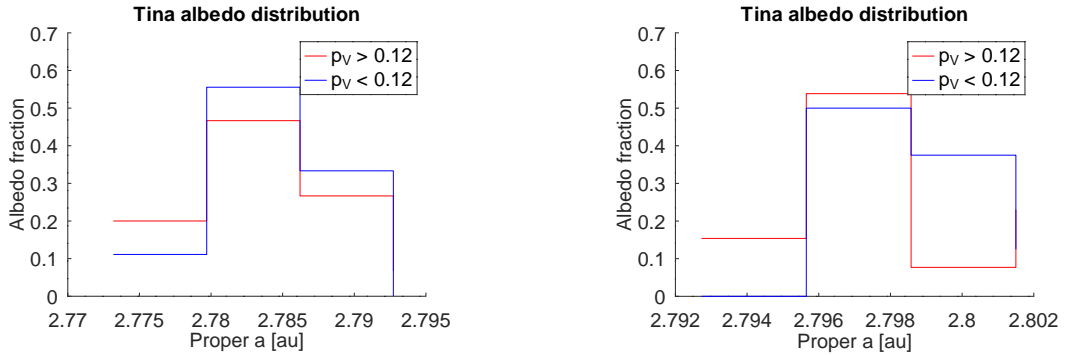


**Figure 15.** The percental distribution of low (blue curve,  $p_V < 0.12$ ) and high (red curve,  $p_V > 0.12$ ) albedo asteroids in the left and right sides of the Tina family V-shape.

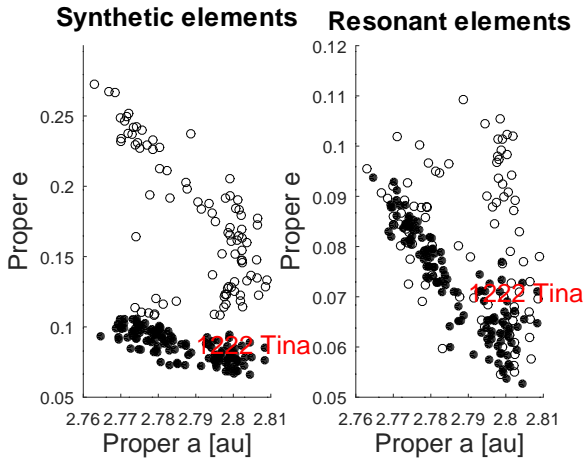


**Figure 16.** On the left panel we display the projection in the synthetic proper ( $a, e$ ) domain of Tina family members, as obtained with HCM, and other anti-aligned asteroids at higher eccentricity in the same stable island. Tina family members are shown as full black dots, while the other asteroids are shown as black circles. The right panel displays the position of the same asteroids in the synthetic proper element ( $a, e$ ) domain. The position of 1222 Tina itself is identified by the red label.

for the information they can provide on the orbital evolution caused by Yarkovsky effect and for the independent constraints on the age and ejection velocity fields that can be inferred from their dynamical configurations.

Using a barrage of methods involving artificial neural networks (ANN), clustering methods, supervised machine learning approaches optimized through the use of genetic algorithms, we were able to obtain a sample of 15 asteroids on aligned orbits and 1669 asteroids on anti-aligned orbits, the largest database so far for this asteroidal population. We obtain the largest sample of resonant arguments images ever produced, with 10004 images, which may be quite valuable for future studies of automatic ANN recognitions of asteroid resonant behavior (Carruba et al. 2021b). We retrieved the three known families crossed by the  $\nu_6$  resonance: the Tina, Euphrosyne, and Svea groups. Two new asteroid groups were identified for the first time in this work: those of Tiffanykapler in the inner main-belt and of 138605 QW177 in the outer belt. Both are completely made of anti-aligned asteroids, which makes them only the second and third groups to have this property, after the Tina family. The Tiffanykapler group is a young asteroid family with an age of  $3.0 \pm 1.2$  Myr, confirmed by two independent dating methods based on time-reversal numerical integration, the Backward Integration Method (BIM) and the Close Encounters Method (CEM). The unique resonant configuration of the Tiffanykapler family, and conserved quantities of the  $\nu_6$  secular resonance allow setting constraints on the family ejection velocity field parameter, with a value of  $V_{\text{EJ}} = 15^{+6}_{-3}$  m/s. This is the first-ever identified young family in the  $\nu_6$  secular resonance, and only the second group, after the Zelima sub-family (Tsirvoulis 2019), for which accurate estimates on the family age and original ejection velocity field can both

be obtained. As more numerous databases of asteroid proper elements are produced, we expect that more and more young asteroid families will be encountered, as recently observed for the Zelima and Tiffanykapler groups.

A new sample of high- $e$  asteroids near the Tina dynamical family was also observed in this work. These objects become connected to the rest of the Tina family at a higher velocity cutoff when using HCM in the domain of resonant elements. This behavior, and the comparable values of albedos of these objects with the rest of the Tina family suggest that they could belong to the first “resonant halo” ever observed in the main-belt. They would be part of an extended Tina family not detectable with standard HCM methods, which is truncated by the dimensions of the local stable island. We identify one possible halo object likely to become unstable on short timescales, which could be an example of ongoing dynamical erosion of an asteroid family.

Finally, we showed that the distribution of Tina’s objects at low albedo ( $p_V < 0.12$ ) in proper  $a$  satisfies the null hypothesis of compatibility with the distribution of objects at high albedo ( $p_V > 0.12$ ) when a Kolmogorov-Smirnov test is applied. This suggests that the two populations are compatible with a common origin. The Tina family could be characterized by a rather unique albedo distribution among X-type asteroid families.

## ACKNOWLEDGMENTS

We thank an anonymous reviewer for valuable comments and suggestions. This research has made use of the Asteroid Families Portal maintained at the Department of Astronomy/University of Belgrade. We would like to thank the Brazilian National Research Council (CNPq, grant 301577/2017-0), the Foundation for Research Support of São Paulo state (FAPESP, grant 2016/024561-0), and the Coordination for the Improvement of Higher Education Personnel (CAPES, grant 88887.374148/2019-00). This is a publication from the MASB (Machine-learning applied to small bodies, <https://valeriocarruba.github.io/Site-MASB/>) research group. Questions on this paper can also be sent to the group email address: [mlasb2021@gmail.com](mailto:mlasb2021@gmail.com).

## 12 DATA AVAILABILITY

A database of the population of asteroids on aligned and anti-aligned libration states of the  $\nu_6$  secular resonance providing information on the identification, proper elements, and physical properties of the asteroids identified in this work will be submitted to the VizieR database (<https://vizier.u-strasbg.fr/viz-bin/VizieR>) if this paper will pass the journal revision process.

## 13 CODE AVAILABILITY

The codes used for the image classification (Carruba et al. 2021b) and identification of family members among the multi- opposition asteroids (Carruba et al. 2020b) are publically available at these GitHub repositories:

- (i) [https://github.com/valeriocarruba/ANN\\_Classification\\_of\\_-M12\\_resonant\\_argument\\_images](https://github.com/valeriocarruba/ANN_Classification_of_-M12_resonant_argument_images)
- (ii) <https://github.com/valeriocarruba/Machine-learning-classification-of-new-asteroid-families-members>

## REFERENCES

Beaugé C., Roig F., 2001, *Icarus*, **153**, 391  
 Bendjoya P., Zappalà V., 2002, in , Asteroids III. Arizona Univ. Press, pp 613–618  
 Bottke W. F., Jedicke R., Morbidelli A., Petit J.-M., Gladman B., 2000, *Science*, **288**, 2190  
 Brož M., 1999, Master’s thesis, Charles University in Prague  
 Brož M., Morbidelli A., 2013, *Icarus*, **223**, 844  
 Brož M., Vokrouhlický D., 2008, *MNRAS*, **390**, 715  
 Carruba V., 2010a, *MNRAS*, **403**, 1834  
 Carruba V., 2010b, *MNRAS*, **408**, 580  
 Carruba V., Morbidelli A., 2011, *MNRAS*, **412**, 2040  
 Carruba V., Domingos R. C., Nesvorný D., Roig F., Huaman M. E., Souami D., 2013, *MNRAS*, **433**, 2075  
 Carruba V., Aljbaae S., Souami D., 2014, *ApJ*, **792**, 46  
 Carruba V., Vokrouhlický D., Novaković B., 2018, *Planet. Space Sci.*, **157**, 72  
 Carruba V., Spoto F., Barletta W., Aljbaae S., Fazenda Á. L., Martins B., 2020a, *Nature Astronomy*, **4**, 83  
 Carruba V., Aljbaae S., Domingos R. C., Lucchini A., Furlaneto P., 2020b, *MNRAS*, **496**, 540  
 Carruba V., Aljbaae S., Domingos R. C., 2021a, *CM&DA*, **133**, 24  
 Carruba V., Aljbaae S., Domingos R. C., Barletta W., 2021b, *MNRAS*, **504**, 692  
 Chen, P. W. and Wang, J. Y. and Lee H. 2004, in 2004 IEEE international joint conference on neural networks (IEEE Cat No04CH37541), pp 2035–2040  
 DeMeo F. E., Carry B., 2013, *Icarus*, **226**, 723  
 Huaman M., Roig F., Carruba V., Domingos R. C., Aljbaae S., 2018, *MNRAS*, **481**, 1707  
 Ivezić Ž., et al., 2001, *AJ*, **122**, 2749  
 Jones R. L., Jurić M., Ivezić Z., 2015, *Proc. Int. Astron. Union*, **10**, 282–292  
 Knežević Z., Milani A., 2003, *A&A*, **403**, 1165  
 Knežević Z., Milani A., Farinella P., Froeschle C., Froeschle C., 1991, *Icarus*, **93**, 316  
 Levison H. F., Duncan M. J., 1994, *Icarus*, **108**, 18  
 Masiero J. R., Mainzer A. K., Grav T., Bauer J. M., Cutri R. M., Nugent C., Cabrera M. S., 2012, *ApJ*, **759**, L8  
 Morbidelli A., 1993, *Icarus*, **105**, 48  
 Morbidelli A., Henrard J., 1991, *CM&DA*, **51**, 169  
 Nesvorný D., Bottke William F. J., Dones L., Levison H. F., 2002, *Nature*, **417**, 720  
 Pedregosa F., et al., 2011, Journal of Machine Learning Research, **12**, 2825  
 Pravec P., et al., 2010, *Nature*, **466**, 1085  
 Radović V., Novaković B., Carruba V., Marčeta D., 2017, *MNRAS*, **470**, 576  
 Ryan E. L., Woodward C. E., 2010, *AJ*, **140**, 933  
 Smirnov N. V., 1939, Bulletin Moscow University, **2**, 3  
 Spoto F., Milani A., Knežević Z., 2015, *Icarus*, **257**, 275  
 Tsirvoulis G., 2019, *MNRAS*, **482**, 2612  
 Usui F., et al., 2011, *PASJ*, **63**, 1117  
 Vokrouhlický D., Brož M., Bottke W. F., Nesvorný D., Morbidelli A., 2006a, *Icarus*, **182**, 118  
 Vokrouhlický D., Brož M., Bottke W. F., Nesvorný D., Morbidelli A., 2006b, *Icarus*, **183**, 349  
 Yoshikawa M., 1987, *CM&DA*, **40**, 233

This paper has been typeset from a  $\text{\TeX}/\text{\LaTeX}$  file prepared by the author.